courses of aggregation during subsequent storage were describable with the empirical Kohlrausch-Williams-Watts (KWW) equation, thus leading to speculation that there were protein molecules having different conformations resulting from stresses during the freeze-drying process, each aggregating with a different time constant (10,14). The temperature dependence of the aggregation rate measured at the initial stage changed around T_{mc} (T_g determined by NMR relaxation measurement (15)), showing an apparent correlation between aggregation rate and structural relaxation (10). In this study, the significance of local obility in aggregation of lyophilized β-GA was examined in comparison with that of structural relaxation. The aggregation rates of β-GA lyophilized with trehalose, sucrose or stachyose were measured at temperatures near T_g, and correlations were examined between aggregation rate and local mobility (as measured by solid-state NMR), T_g (a primary parameter of structural relaxation), or protein conformational changes (as measured by FT-IR).

MATERIALS AND METHODS

Preparation of Lyophilized β-GA Formulations

β-GA from Aspergillus oryzae (10 U/mg; molecular weight: 105,000; isoelectric point:4.6) was kindly provided by Amano Enzyme Inc. (Nagoya, Japan) and purified by dialysis against 2.5 mM sodium phosphate solution of pH 4.5 (adjusted with HCl). After concentrated by ultrafiltration, trehalose (203-02252, Wako Pure Chemical Ind. Ltd, Osaka, Japan), sucrose (S-9378, Sigma Chemical Co., St. Louis, MO, USA) or stachyose (S-4001, Sigma Chemical Co., St. Louis, MO, USA) solution was added to make a 3.3 mg/ml β-GA solution with various weight fractions of excipient. Two hundred microliters of the solution was frozen in a polypropylene sample tube (2.0 ml) by immersion in liquid nitrogen for 10 min, and then dried at a vacuum level below 5 Pa for 23.5 h in a lyophilizer (Freezevac C-1, Tozai Tsusho Co., Tokyo, Japan). The shelf temperature was between −35 and −30°C for the first 10 h, 20°C for the subsequent 10 h, and 30°C for the last 3.5 h.

Determination of Water Sorption and T_g of Lyophilized β-GA Formulations

Water vapor absorption isotherms were measured gravimetrically at 25°C for lyophilized β-GA formulations containing trehalose, sucrose or stachyose using the automated sorption analyzer (MB-300 G system, VTI Corp., FL, USA). Samples were dried at 25°C under a vacuum level below 0.1 Pa until changes in weight were less than 1 μg per 10 min. Water contents of the samples at partial vapor pressures of 0.10 and 0.20 (corresponding to 10 and 20% relative humidity (RH), respectively) were determined based on equilibrated sample weight (changes in weight of less than 1 μg per 10 min).

The T_g of lyophilized β-GA formulations was determined by modulated temperature differential scanning calorimetry (2920; TA Instruments, DE, USA). Before T_g measurements, samples were stored at 15°C for 24 h in a desiccator with a saturated solution of LiCl H_2O (12% RH). The conditions were as follows: modulation period of 100 s, a modulation amplitude of ±0.5°C, and an underlying heating rate of 1°C/min. Samples were put in a hermetic pan. Temperature calibration was performed using indium.

Determination of $T_{1\rho}$ of β-GA Carbonyl Carbon by ^{13}C Solid-state NMR

The rotating-frame spin-lattice relaxation time ($T_{1\rho}$) of β-GA carbonyl carbon in lyophilized formulations containing various weight fractions of trehalose, sucrose and stachyose was determined at 25°C using a UNITY plus spectrometer operating at a proton resonance frequency of 400 MHz (Varian Inc., CA, USA). Lyophilized samples were pre-equilibrated at 12% RH. Spin-locking field was equivalent to 19 kHz. The rotor size was 7 mm and spinning speed was 4 kHz. Peak height at approximately 180 ppm due to β-GA carbonyl carbon was followed with delay times of 1, 5, 10, 20, 30, 50 and 80 ms. Similar measurement of $T_{1\rho}$ was performed for lyophilized β-GA alone.

Fourier Transform Infra Red (FT-IR) Spectroscopy Measurements

FT-IR spectroscopy was performed using a JASCO FT/IR-6300 spectrometer (JASCO, Tokyo, Japan). A mixture of 100 mg KBr and 1–2 mg lyophilized β-GA formulation was pressed into a pellet under vacuum. A total of 256 scans and a resolution of 4 cm^{-1} were used for each spectrum. The second-derivative spectra were obtained from intact spectra without smoothing using Spectra Manager software version 2 (JASCO, Tokyo, Japan). The area of spectral absorbance was calculated using a baseline drawn between 1,600 and 1,700 cm^{-1}, and normalized for comparison between the formulations containing different excipients.

Determination of β-GA Aggregation Rate in Lyophilized Formulations

Lyophilized β-GA formulations containing trehalose, sucrose or stachyose, pre-equilibrated at 12% RH, were stored with a tight screw-cap at a constant temperature (40–90°C), removed at various times, and stored in liquid nitrogen until assayed. Samples were reconstituted in 1.7 ml of 200 mM phosphate buffer (pH 6.2), and injected into a size exclusion chromatography as described previously (10). The column (Tosoh G3000SW, 30 cm×7.5 mm, Tokyo) was maintained at 30°C, and 200 mM phosphate buffer (pH 6.2) was used as the mobile phase. The detection wavelength was 280 nm. Monomeric β-GA was determined based on the peak height of its chromatogram.

Reconstitution of lyophilized β-GA formulations after storage was also carried out using reconstitution mediums of 200 mM phosphate buffer (pH 6.2) containing 0.5% additives (dextran sulfate (197-08362, Wako Pure Chemical Ind. Ltd, Osaka, Japan), 2-hydroxylpropyl-β-cyclodextrin (C-0926, Sigma Chemical Co.), poly-L-lysine (P-7890, Sigma Chemical Co.), or pluronic (F-68, P-7061, Sigma Chemical Co., St. Louis, MO, USA).

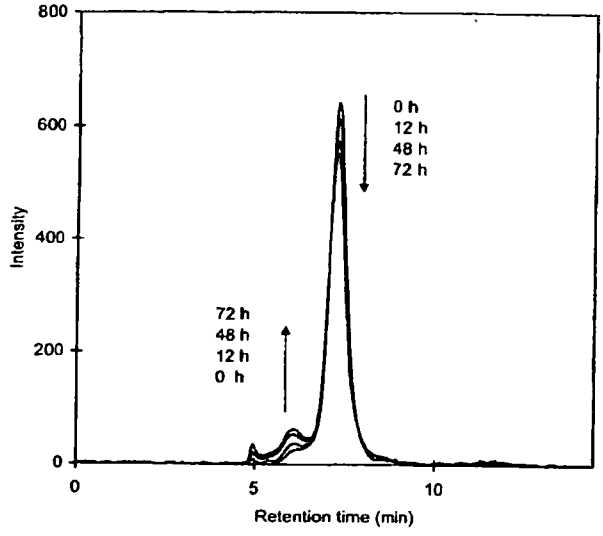

Fig. 1. Size-exclusion chromatograms of β-GA lyophilized with trehalose after various periods of storage at 80°C and 12%RH. The weight fraction of trehalose : 0.5.

RESULTS AND DISCUSSION

Aggregation of β-GA during Storage of Lyophilized Formulations

Figure 1 shows representative size-exclusion chromatograms of β-GA in lyophilized formulations, indicating that monomeric β-GA aggregates to larger sizes during storage. Tables I and II show the effects of reconstitution medium on the amount of monomeric β-GA remaining after storage of the formulation containing trehalose at temperatures below and above T_g, respectively. The amount of monomeric β-GA was not significantly affected by the addition of dextran sulfate or poly-L-lysine. Addition of pluronic also had no significant effect on the amount of monomeric β-GA. For lyophilized interleukin-2, the amount of aggregates after reconstitution was decreased by addition of poly-ions with high charge density, such as dextran sulfate and poly-L-lysine, and increased by addition of surfactants, such as pluronic, into the reconstitution buffer solution (16). This may be explained by assuming that the formation of aggregates from partially unfolded intermediates, as well as the reverse formation of native protein from intermediates, occur during the reconstitution process. In contrast, the lack of the effects of additives observed for β-GA aggregation indicates that neither formation of aggregates nor reverse formation of native protein from partially unfolded intermediates occurs during the reconstitution process. This finding suggests that β-GA aggregation occurs during the storage of lyophilized formulations, even at temperatures below T_g. Because large-scale diffusion of protein molecules is considered to be very limited in glassy solids, β-GA aggregation is considered to occur between protein molecules that are adjacent to each other without large-scale diffusion.

Temperature Dependence of β-GA Aggregation Rate

Figure 2 shows time courses of aggregation of β-GA at 50°C (below T_g) for lyophilized formulations with an excipient fraction of 0.33, and at 80°C (above T_g) for lyophilized formulations with an excipient fraction of 0.5. Similar time courses were obtained for formulations with various excipient fractions and at various temperatures. The wide range of the time courses could be better described by the KWW equation, but the initial stages of aggregation were describable with first-order kinetics. The solid line in Fig. 2 represents the theoretical time course of first-order kinetics.

The time required for 10% degradation (t_{90}) was calculated from the apparent first-order rate constant. Figure 3 shows the temperature-dependence of t_{90} determined for aggregation of β-GA lyophilized with sucrose, trehalose or stachyose at an excipient fractions of 0.33 and 0.5, 12% RH and various temperatures. For the sucrose and trehalose formulations, the temperature dependence of t_{90} exhibited a change in the slope at around T_g, suggesting significant effects of molecular mobility. For the stachyose formulation, the change in the slope was not obvious, because few data were available at temperatures above T_g. The values of t_{90} at T_g largely depended on the excipient; sucrose > trehalose > stachyose. The finding that the t_{90} values at T_g varied significantly between these three formulations suggests that β-GA aggregation rate is not primarily related to ($T-T_g$).

Table I. Effects of Reconstitution Medium on β-GA Aggregation Below T_g for 0.09 Trehalose Formulation

Additives in Reconstitution Medium	Peak Height for Monomeric β-GA (Relative to Solution Prior to Freeze Drying)			
	After Freeze Drying		After 24 h-storage at 70°C	
None	0.97	(0.01)	0.65	(0.01)
Dextran Sulfate	0.96	(0.00)	0.62	(0.01)
2-hydroxylpropyl-β-cyclodextrin	0.95	(0.01)	0.62	(0.00)
Poly-L-lysine	0.94	(0.01)	0.62	(0.00)
Pluronic	0.97	(0.01)	0.66	(0.01)

0.5% additives
Values in brackets represent standard deviation (n=3)

Table II. Effects of Reconstitution Medium on β-GA Aggregation Above T_g for 0.33 Trehalose Formulation

Additives in Reconstitution Medium	Peak Height for Monomeric β-GA (Relative to Solution Prior to Freeze Drying)			
	After Freeze Drying		After 9 h-storage at 90°C	
None	0.99	(0.01)	0.74	(0.03)
Dextran Sulfate	1.00	(0.00)	0.74	(0.01)
2-hydroxylpropyl-β-cyclodextrin	0.98	(0.00)	0.73	(0.01)
Poly-L-lysine	0.98	(0.01)	0.74	(0.01)
Pluronic	1.00	(0.01)	0.76	(0.02)

0.5% additives
Values in brackets represent standard deviation (n=3)

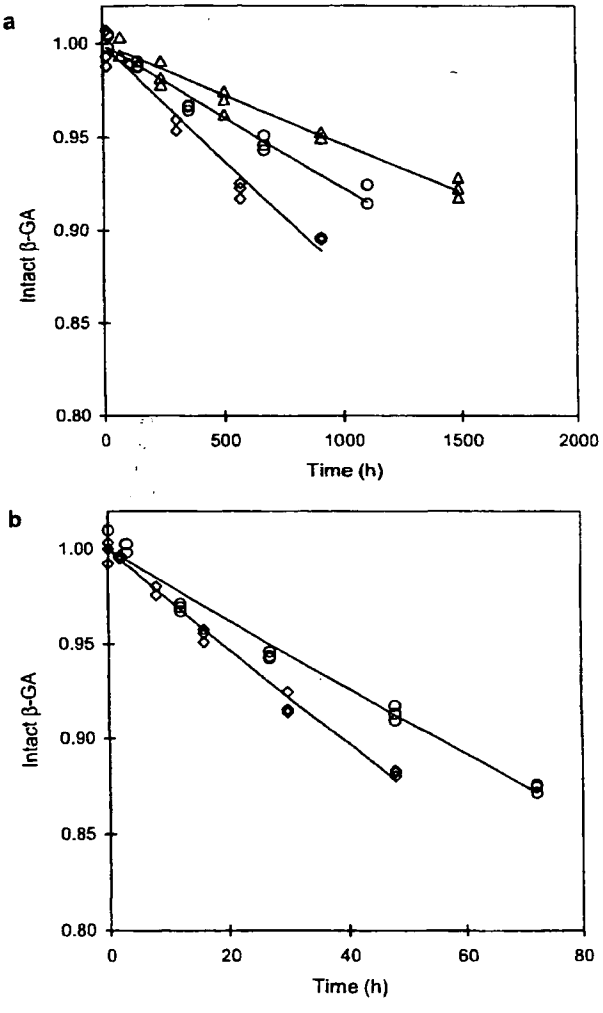

Fig. 2. Time courses of aggregation of β-GA lyophilized with sucrose (△), trehalose (○) or stachyose (◇). (a) aggregation at 50°C and excipient fraction of 0.33. (b) aggregation at 80°C and excipient fraction of 0.5.

Excipient-Fraction Dependence of β-GA Aggregation Rate

Figure 4 shows the dependence of t_{90} on the weight fraction of excipient at temperatures below T_g (50°C) and above T_g (80°C). As the weight fraction of excipient increased, t_{90} increased for all formulations. The values of t_{90} for the sucrose formulation in the amorphous state could not be determined at fractions above 0.5 at 50°C or above 0.33 at 80°C, because crystallization occurred during storage (crystallization was confirmed by the lack of crystallization peak in DSC thermograms). The t_{90} observed for β-GA aggregation showed a log-linear dependence on the excipient fraction, as reported for other proteins (11,12).

Figure 5 shows the water content and T_g determined for the lyophilized β-GA formulations with various weight fractions of trehalose, sucrose or stachyose. It has often been reported that lyophilized proteins without excipients do not show a distinct change in heat capacity in DSC thermograms. The T_g of lyophilized β-GA alone could not be determined in the dry state, but it could be estimated at 12% RH from small changes in heat capacity (Fig. 6). The T_g value determined at 12% RH depended on the excipient fraction (Fig. 5); T_g decreased with increasing excipient fraction from 0 to 0.3. Only a single T_g was observed in the range of excipient fractions from 0 to 0.3 for all formulations, suggesting that these formulations are a single glassy phase on levels detectable by DSC.

As shown in Figs. 4 and 5, the rank order of t_{90} at a certain excipient fraction was sucrose > trehalose > stachyose, whereas that of T_g of β-GA formulations was sucrose < trehalose < stachyose. The value of t_{90} increased significantly with increasing excipient fraction, even at small excipient fractions, in which T_g decreased significantly with increasing excipient fraction. These findings indicate that β-GA aggregation rate is not primarily related to $(T-T_g)$.

Figure 7 shows the amount of monomeric β-GA remaining after freeze drying with sucrose, trehalose or stachyose. Significant changes were observed at an excipient fraction of 0.09 for all formulations. The stachyose formulation exhibited the largest degree of β-GA aggregation during freeze drying. This finding suggests that freeze-drying processes cause changes in protein conformation at differing degrees between excipients, which in turn leads to the differences in β-GA aggregation rate observed between excipients. FT-IR is known to be useful for detecting changes in protein conformation produced during the freeze-drying process (17). Figure 8 compares the second derivative FT-IR

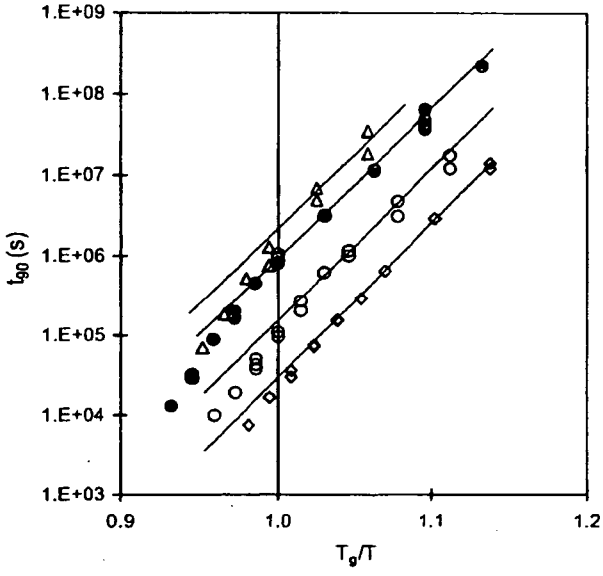

Fig. 3. T/T_g-dependence of t_{90} for aggregation of β-GA lyophilized with sucrose (△), trehalose (○●) or stachyose (◇). The weight fraction of excipient : 0.33 (△○◇) and 0.5 (●).

spectra between the sucrose, trehalose and stachyose formulations. Significant differences in spectra were not observed between the excipients, and the differences in β-GA aggregation rate observed between the excipients could not be attributed to differences in protein secondary structure. It is known that changes in the tertiary structure of protein molecules created during freeze-drying processes can lead to

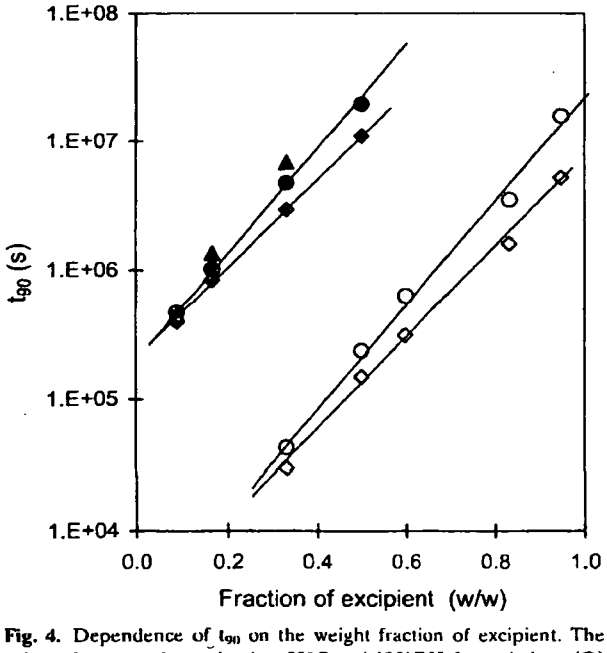

Fig. 4. Dependence of t_{90} on the weight fraction of excipient. The value of t_{90} was determined at 80°C and 12%RH for trehalose (○) and stachyose (◇), and at 50°C and 12%RH for trehalose (●), sucrose (▲) and stachyose (◆).

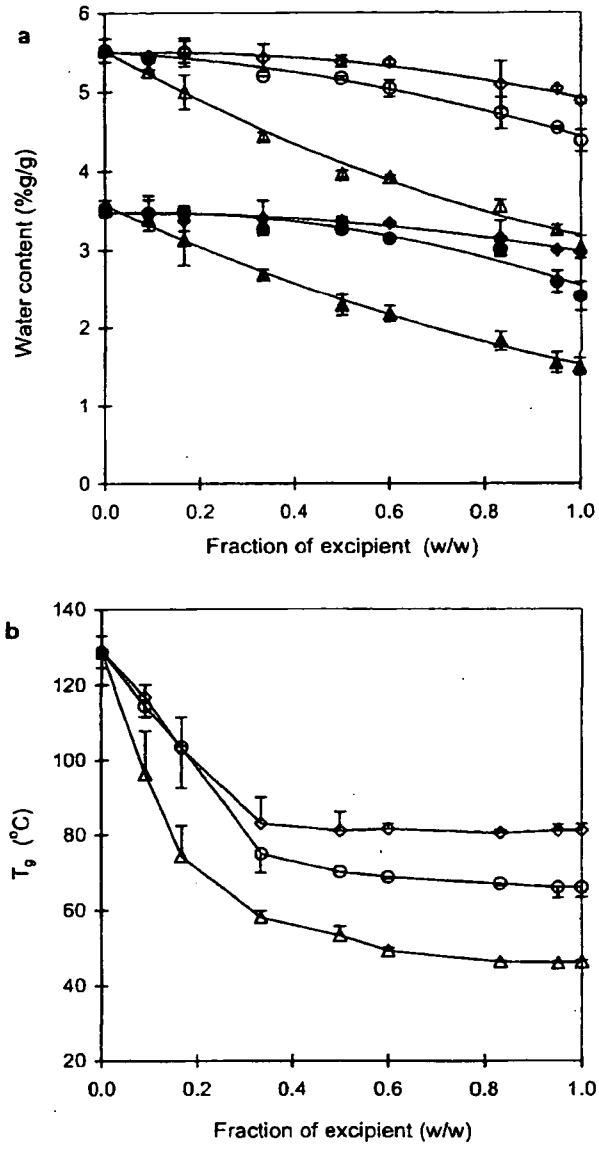

Fig. 5. Water content (a) and T_g (b) of lyophilized β-GA formulations containing trehalose (○●), sucrose (△▲), or stachyose (◇◆) as a function of the weight fraction of excipient. (a) *closed symbols*: 10%RH; *open symbols*: 20%RH. 25°C. (b) 12%RH. sd (n=3).

protein aggregation during storage. A possibility that a tertiary structural change is responsible for the differences in β-GA aggregation rate observed between the excipients cannot be excluded.

Significance of Local Mobility, as Determined by $T_{1\rho}$ of β-GA Carbonyl Carbon, and Structural Relaxation in Protein Aggregation

It is generally considered that the rate of protein aggregation, an intermolecular reaction, is mainly determined by structural relaxation that allows for large-scale

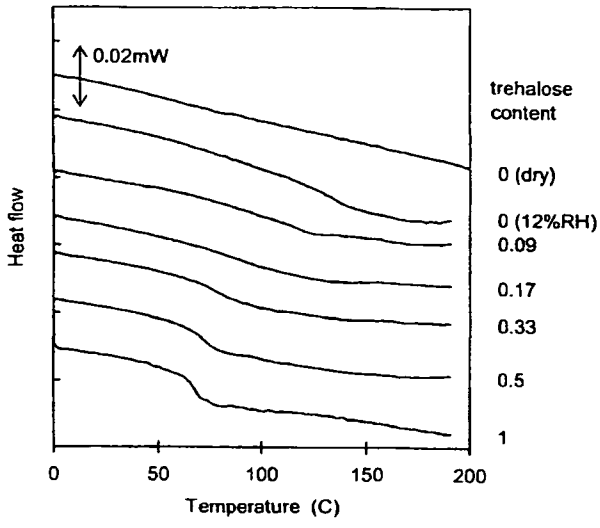

Fig. 6. DSC thermogram for β-GA lyophilized with various weight fractions of trehalose.

diffusion of reactants. From the finding that the t_{90} versus T_g/T plots for the lyophilized β-GA formulations exhibited a change in slope around T_g, β-GA aggregation rate appeared to correlate with structural relaxation. Although β-GA aggregation rate was not related to $(T-T_g)$, this may be explained by assuming that the fragility and fictive temperature of the formulation vary with the excipient. Because the structural relaxation times of the β-GA formulations were not determined in this study, correlations between β-GA aggregation rate and structural relaxation could not be elucidated.

Meanwhile, the local mobility of β-GA was determined by $T_{1\rho}$ of β-GA carbonyl carbon. Figure 9 shows the time course of rotating-frame spin-lattice relaxation at 25°C and 12% RH for the carbonyl carbon of β-GA lyophilized with sucrose, trehalose or stachyose at an excipient fraction of 0.5.

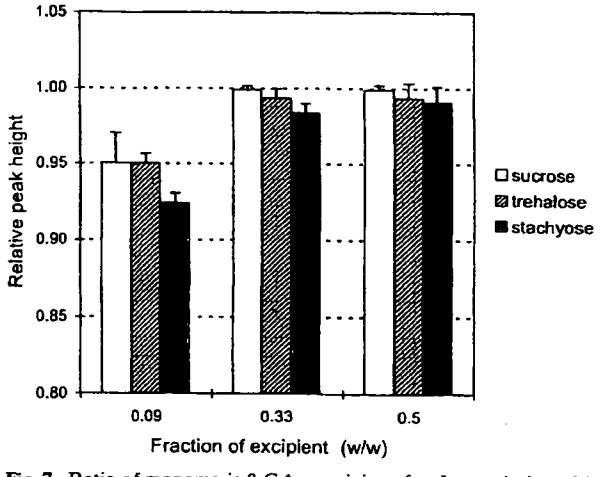

Fig. 7. Ratio of monomeric β-GA remaining after freeze drying with sucrose, trehalose or stachyose. *Bars* represent standard deviation (n=3).

Spin-lattice relaxation was significantly retarded by the addition of excipient. Sucrose resulted in the largest degree of retardation, and there were no significant differences in the degree of retardation between the trehalose and stachyose formulations. The time course of spin-lattice relaxation was describable with a bi-exponential equation including two different $T_{1\rho}$ values. The longer $T_{1\rho}$ value was estimated by curve fitting using a shorter $T_{1\rho}$ of 9 ms and a proportion of 13% for carbonyl carbons with the shorter $T_{1\rho}$. Figure 10 shows the estimates for the longer $T_{1\rho}$ of the dominating proportion, plotted as a function of the excipient fraction. The $T_{1\rho}$ for the sucrose formulation increased significantly with excipient fraction. For the stachyose formulation, in contrast, increases in $T_{1\rho}$ were not significant at an excipient fraction of 0.09, and $T_{1\rho}$ was less than in the sucrose formulation at higher excipient fractions. $T_{1\rho}$ for the trehalose formulation exhibited intermediate behavior when compared to the sucrose and stachyose formulations. The rank order of the ability of excipients to decrease the local

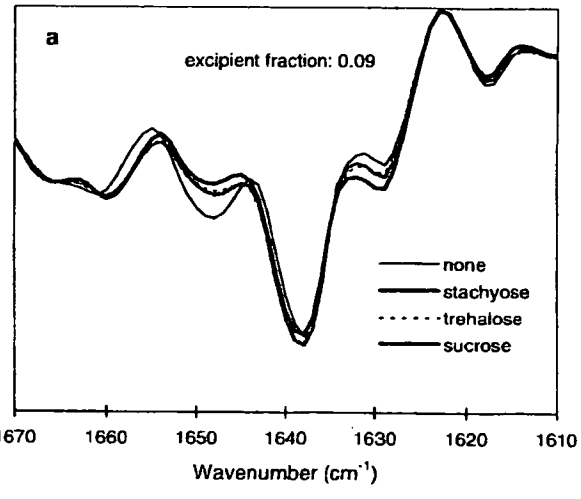

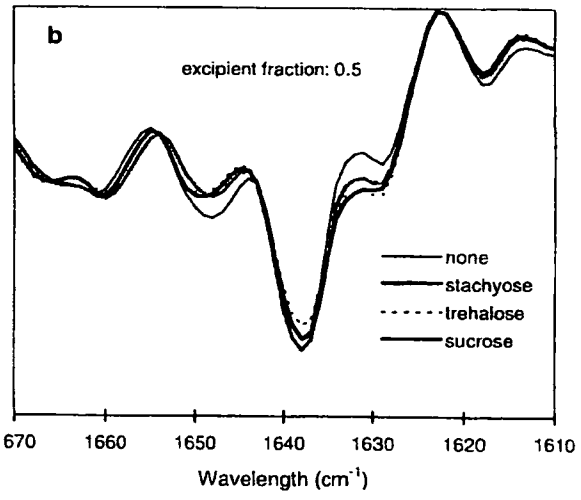

Fig. 8. Second derivative FT-IR spectra for β-GA lyophilized with sucrose, trehalose or stachyose of 0.09 (a) and 0.5 fractions (b).

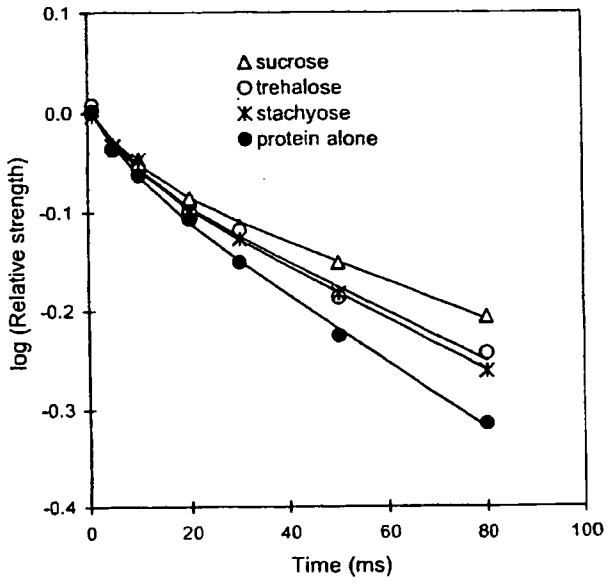

Fig. 9. Time course of spin-lattice relaxation at 25°C and 12%RH for carbonyl carbon of β-GA lyophilized with sucrose, trehalose or stachyose. The weight fraction of excipient : 0.5.

mobility of β-GA appeared to be the same as the rank order of their ability to decrease aggregation rate. This finding suggests that local mobility is a primary factor that affects the stability of lyophilized β-GA formulations; sucrose more potently inhibits local mobility of β-GA, and thus more strongly inhibits β-GA aggregation.

Local mobility is generally considered to follow Arrhenius kinetics. If local mobility is mainly responsible for β-GA aggregation, the temperature dependence of t_{90} should not show a change in slope around T_g. The non-Arrhenius temperature dependence observed for the t_{90} of β-GA aggregation, which is considered to be governed by local mobility, may be explained by assuming that local mobility of protein is coupled with structural relaxation. For bovine serum γ-globulin, the local mobility of protein, as measured by the laboratory-frame spin-lattice relaxation time (T_1) of protein carbonyl carbon, exhibited Arrhenius temperature dependence when lyophilized without excipient (18). When lyophilized with dextran, in contrast, the local mobility of protein exhibited a change in the slope of temperature dependence around the T_{mc} (T_g determined by NMR relaxation measurement), as did local mobility of dextran, as measured by T_1 of dextran methine carbon. These findings suggested that the local mobility of protein was coupled with the structural relaxation of lyophilized solids. The same may be said for the local mobility of protein and structural relaxation of β-GA lyophilized with sucrose, trahalose or stachyose. The local mobility of β-GA may exhibit Arrhenius temperature dependence in the absence of excipient. Upon the addition of excipient, local mobility may become to be coupled with structural relaxation, and the temperature dependence of protein local mobility may become to deviate from Arrhenius behavior.

The great increase in t_{90} with increasing excipient fraction observed for β-GA aggregation rate, as indicated by log-linear dependence on the excipient fraction, may be attributed mainly to the effect of excipient inhibiting protein local mobility in addition to the effect of excipient diluting protein molecules.

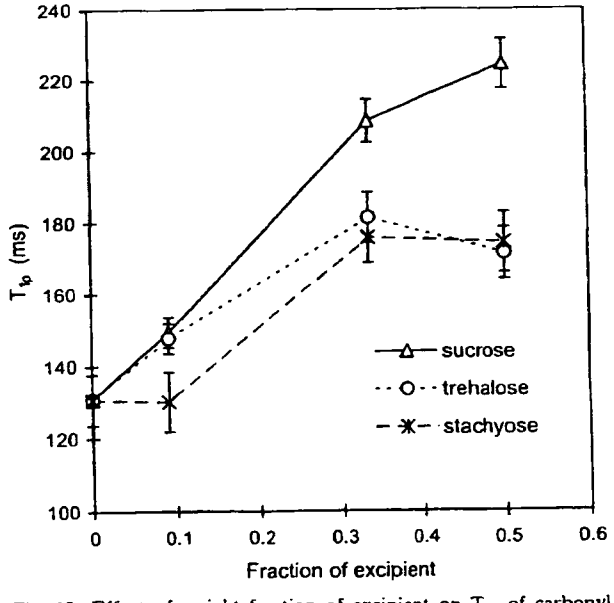

Fig. 10. Effect of weight fraction of excipient on $T_{1\rho}$ of carbonyl carbon at 25°C and 12%RH for β-GA lyophilized with sucrose, trehalose or stachyose

CONCLUSION

The aggregation rate of β-GA lyophilized with sucrose, trehalose or stachyose unexpectedly correlated with the local mobility of β-GA rather than with ($T-T_g$). An increase in the weight fraction of excipient appeared to increase the effects of excipient decreasing local mobility, resulting in increases in the stability of β-GA. Sucrose exhibited the most intense stabilizing effect due to the most intense ability to inhibit local protein mobility during storage.

REFERENCES

1. M. J. Pikal. Chemistry in solid amorphous matrices: implication for biostabilization. In H. Levine (ed.), *Amorphous Food and Pharmaceutical Systems*, The Royal Society of Chemistry, Cambridge, UK, 2002, pp. 257–272.
2. S. Yoshioka, and Y. Aso. Correlations between molecular mobility and chemical stability during storage of amorphous pharmaceuticals. *J. Pharm. Sci.* in press (2006).
3. M. J. Pikal, K. M. Dellerman, M. L. Roy, and R. M. Riggin. The effects of formulation variables on the stability of freeze-dried human growth hormone. *Pharm. Res.* 8:427–436 (1991).
4. C. Schebor, M. P. Buera, and J. Chirife. Glassy state in relation to thermal inactivation of the enzyme invertase in amorphous dried matrices of trehalose, maltodextrin and PVP. *J. Food Eng.* 30:269–282 (1996).
5. S. J. Prestrelski, K. A. Pikal, and T. Arakawa. Optimization of lyophilization conditions for recombinant human interleukin-2

by dried-state conformational analysis using fourier-transform infrared spectroscopy. *Pharm. Res.* **12**:1250–1259 (1995).
6. S. Yoshioka, Y. Aso, and S. Kojima. Dependence of molecular mobility and protein stability of freeze-dried γ-globulin formulations on the molecular weight of dextran. *Pharm. Res.* **14**:736–741 (1997).
7. S. P. Duddu, and P. R. Dal Monte. Effect of glass transition temperature on the stability of lyophilized formulations containing a chimeric therapeutic monoclonal antibody. *Pharm. Res.* **14**:591–595 (1997).
8. S. Yoshioka, Y. Aso, and S. Kojima. Determination of molecular mobility of lyophilized bovine serum albumin and γ-globulin by solid state ^{1}H-NMR and relation to aggregation-susceptibility. *Pharm. Res.* **13**:926–930 (1996).
9. S. Yoshioka, Y. Aso, and S. Kojima. Softening temperature of lyophilized bovine serum albumin and γ-globulin as measured by spin-spin relaxation time of protein protons. *J. Pharm. Sci.* **86**:470–474 (1997).
10. S. Yoshioka, S. Tajima, Y. Aso, and S. Kojima. Inactivation and aggregation of β-galactosidase in lyophilized formulation described by Kohlrausch-Williams-Watts stretched exponential function. *Pharm. Res.* **20**:1655–1660 (2003).
11. L. Chang, D. Shepherd, J. Sun, D. Ouellette, K. L. Grant, X. Tang, and M. J. Pikal. Mechanism of protein stabilization by sugars during freeze-drying and storage: native structure preservation, specific interaction, and/or immobilization in a glassy matrix? *J. Pharm. Sci.* **94**:1427–1444 (2005).
12. L. Chang, D. Shepherd, J. Sun, X. Tang, and M. J. Pikal. Effect of sorbitol and residual moisture on the stability of lyophilized antibodies: implications for the mechanism of protein stabilization in the solid state. *J. Pharm. Sci.* **94**:1445–1455 (2005).
13. S. Yoshioka, Y. Aso, S. Kojima, and T. Tanimoto. Effect of polymer excipients on the enzyme activity of lyophilized bilirubin oxidase and β-galactosidase formulations. *Chem. Pharm. Bull.* **48**:283–285 (2000).
14. S. Yoshioka, Y. Aso, and S. Kojima. Usefulness of Kohlrausch-Williams-Watts stretched exponential function to describe protein aggregation in lyophilized formulations and temperature dependence of near the glass transition temperature. *Pharm. Res.* **18**:256–260 (2001).
15. S. Yoshioka, Y. Aso, and S. Kojima. The effect of excipients on the molecular mobility of lyophilized formulations, as measured by glass transition temperature and NMR relaxation-based critical mobility temperature. *Pharm. Res.* **16**:135–140 (1999).
16. M. Z. Zhang, K. Pikal, T. Nguyen, T. Arakawa, and S. J. Prestrelski. The effect of the reconstitution medium on aggregation of lyophilized recombinant interleukin-2 and ribonuclease A. *Pharm. Res.* **13**:643–646 (1996).
17. S. J. Prestrelski, T. Arakawa, and J. Carpenter. Separation of freezing- and drying-induced denaturation of lyophilized proteins using stress-specific stabilization. *Arch. Biochem. Biophys.* **303**:465–473 (1993).
18. S. Yoshioka, Y. Aso, S. Kojima, S. Sakurai, T. Fujiwara, and H. Akutsu. Molecular mobility of protein in lyophilized formulations linked to the molecular mobility of polymer excipients, as determined by high resolution ^{13}C solid-state NMR. *Pharm. Res.* **16**:1621–1625 (1999).

Available online at www.sciencedirect.com
ScienceDirect
International Journal of Pharmaceutics 336 (2007) 191–195
INTERNATIONAL JOURNAL OF PHARMACEUTICS
www.elsevier.com/locate/ijpharm

Note

Crystallization rate of amorphous nifedipine analogues unrelated to the glass transition temperature

Tamaki Miyazaki *, Sumie Yoshioka, Yukio Aso, Toru Kawanishi

National Institute of Health Sciences, 1-18-1 Kamiyoga, Setagaya-ku, Tokyo 158-0851, Japan

Received 14 August 2006; received in revised form 12 October 2006; accepted 18 November 2006
Available online 28 November 2006

Abstract

To examine the relative contributions of molecular mobility and thermodynamic factor, the relationship between glass transition temperature (T_g) and the crystallization rate was examined using amorphous dihydropyridines (nifedipine (NFD), *m*-nifedipine (*m*-NFD), nitrendipine (NTR) and nilvadipine (NLV)) with differing T_g values. The time required for 10% crystallization, t_{90}, was calculated from the time course of decreases in the heat capacity change at T_g. The t_{90} of NLV and NTR decreased with decreases in T_g associated with water sorption. The t_{90} versus T_g/T plots almost overlapped for samples of differing water contents, indicating that the crystallization rate is determined by molecular mobility as indicated by T_g. In contrast, differences in the crystallization rate between these four drugs cannot be explained only by molecular mobility, since the t_{90} values at a given T_g/T were in the order: NLV > NTR > NFD ≈ *m*-NFD. A lower rate was obtained for amorphous drugs with lower structural symmetry and more bulky functional groups, suggesting that these factors are also important. Furthermore, the crystallization rate of NTR in solid dispersions with poly(vinylpyrrolidone) (PVP) and hydroxypropyl methylcellulose (HPMC) decreased to a greater extent than expected from the increased T_g. This also suggests that factors other than molecular mobility affect the crystallization rate.
© 2006 Elsevier B.V. All rights reserved.

Keywords: Crystallization; Amorphous state; Nifedipine; Glass transition; Molecular mobility; Excipients

Preparation of poorly water-soluble pharmaceuticals into amorphous forms improves their solubility. However, amorphous solids are physically unstable because of their high energy state, and crystallization during storage presents a problem. The process of crystallization is known to comprise two major steps: nucleation and crystal growth, and the rates are generally governed by molecular mobility affecting the diffusion rate of molecules and thermodynamic factors such as the Gibbs free energy and nucleus/amorphous interfacial energy (Salcki-Gerhardt and Zografi, 1994; Hancock and Zografi, 1997; Rodríguez-Hornedo and Murphy, 1999; Andronis and Zografi, 2000; Ngai et al., 2000). Our previous studies demonstrated that the overall crystallization rate of nifedipine (NFD) for both the amorphous pure drug and solid dispersions with poly(vinylpyrrolidone) (PVP) had similar temperature dependence as the mean relaxation time calculated using the Adam-Gibbs-Vogel equation, suggesting that the molecular mobility of amorphous pharmaceuticals was one of the important factors affecting the crystallization rate (Aso et al., 2001, 2004). However, the crystallization rate of amorphous pharmaceuticals cannot be determined only by molecular mobility, as it has been reported that the susceptibility to crystallization of pharmaceuticals possessing quite different thermodynamic properties does not follow the order of the decrease in the glass transition temperature (T_g) (Zhou et al., 2002).

The purpose of the present study is to discuss the relative contributions of the molecular mobility and thermodynamic factors to the crystallization rates of dihydropyridines with different substituents, including NFD, *m*-nifedipine (*m*-NFD), nitrendipine (NTR) and nilvadipine (NLV) (Fig. 1). The overall crystallization rates of these drugs in the pure amorphous solids were measured under various relative humidity (RH) conditions to elucidate the effects of the substituents and water content on the crystallization rate. The crystallization rate of NTR was also determined in solid dispersions containing polymers (PVP and hydroxypropyl methylcellulose (HPMC)). Although some

* Corresponding author. Tel.: +81 3 3700 1141; fax: +81 3 3707 6950.
E-mail addresses: miyazaki@nihs.go.jp (T. Miyazaki), yoshioka@nihs.go.jp (S. Yoshioka), aso@nihs.go.jp (Y. Aso), kawanish@nihs.go.jp (T. Kawanishi).

0378-5173/$ – see front matter © 2006 Elsevier B.V. All rights reserved.
doi:10.1016/j.ijpharm.2006.11.052

	abbreviation	R_1	R_2	R_3	R_4
nifedipine	[NFD]	CH_3	CH_3	NO_2	H
m-nifedipine	[m-NFD]	CH_3	CH_3	H	NO_2
nitrendipine	[NTR]	CH_3	C_2H_5	H	NO_2
nilvadipine	[NLV]	CN	$(CH_3)_2CH$	H	NO_2

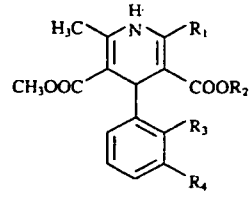

Fig. 1. Chemical structures of dihydropyridines.

papers have dealt with the crystallization of NTR and NLV in solid dispersions (Hirasawa et al., 2003a,b, 2004; Wang et al., 2005, 2006), few data are available that allow quantitative discussion about the relationship between molecular mobility and crystallization rates.

NFD and HPMC (USP grade) were purchased from Sigma Chemical Co. NTR, *m*-NFD and PVP (weight average molecular weight of 40000) were obtained from Wako Pure Chemical Industries Ltd. NLV was kindly supplied by Astellas Pharma Inc. The amorphous NFD, *m*-NFD, NTR, NLV and NTR solid dispersions with PVP and HPMC were prepared by melt quenching in the cell of a differential scanning calorimeter (DSC2920, TA Instruments). The crystalline drug or mixture of NTR and polymer (5 mg) was melted at a temperature approximately 20 °C above its melting point and then cooled to approximately 100 °C below the T_g at a cooling rate of 40 °C/min. Thermal and photo degradation of the drugs was checked by HPLC, and no change in the chromatograms was observed after the preparation in comparison with that before. Fig. 2 shows typical DSC thermograms for the four amorphous drugs immediately after preparation and after subsequent storage. The T_g values for the amorphous drugs were: NLV, 48.6 ± 0.3 °C; NFD, 46.2 ± 0.2 °C; *m*-NFD, 41.3 ± 0.1 °C; NTR, 32.4 ± 0.3 °C. As shown in Fig. 2(b), freshly prepared amorphous NFD exhibited two endothermic peaks at around 161 °C and 168 °C. The two melting points of the peaks agreed well with that for the metastable form II and stable form I, respectively (Burger and Koller, 1996). As shown in Fig. 2(c), the NFD sample, retaining an amorphous portion after 5 h storage at 60 °C, showed exothermic peaks due to crystallization of the amorphous phase and its transformation into a stable crystal, and melted at 168 °C, which is approximately the same temperature as the melting point of the intact crystal. As shown in Fig. 2(d), the sample stored at 60 °C for 46 h showed the exothermic peak around 120–140 °C due to transformation into a stable crystal, although change in the heat capacity (ΔC_p) at T_g was not significant. The exothermic peak around 120–140 °C due to transformation into a stable crystal was also observed during storage at 50 °C and 70 °C (thermogram not shown). These DSC thermograms suggested that amorphous NFD initially crystallized into a metastable form. Crystallization into the metastable form was also observed during storage at 50 °C and 70 °C (thermogram not shown). Amorphous *m*-NFD showed an exothermic peak due to crystallization but no obvious peak due to transformation into a stable form like that shown by the NFD samples, and melted at 206 °C, which is approximately the same temperature as the melting point of intact *m*-NFD (Fig. 2(f) and (g)). It is not clear from the DSC thermograms whether transition to a stable or a metastable crystalline form occurred during storage. Fig. 2(j) and (k) show the DSC thermograms of the partially crystallized NTR samples showing one melting peak at 128 °C. The observed melting point was lower than that of the stable crystal

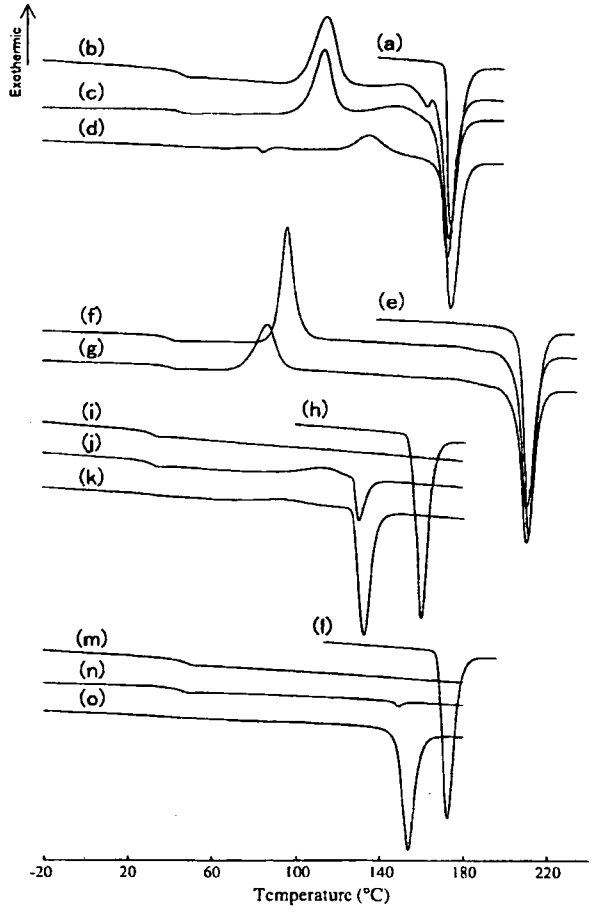

Fig. 2. Typical DSC thermograms: (a) NFD crystalline in the stable form, (b) freshly prepared amorphous NFD, (c) amorphous NFD after 5h-storage at 60 °C (d) amorphous NFD after 46 h-storage at 60 °C, (e) m-NFD crystalline in the stable form, (f) freshly prepared amorphous m-NFD, (g) amorphous m-NFD after 15 h-storage at 50 °C, (h) NTR crystalline in the stable form, (i) freshly prepared amorphous NTR, (j) amorphous NTR after 2 h-storage at 60 °C, (k) amorphous NTR after 9.75 h-storage at 60 °C, (l) NLV crystalline in the stable form, (m) freshly prepared amorphous NLV, (n) amorphous NLV after 48 h-storage at 80 °C, (o) amorphous NLV after 168 h-storage at 80 °C. Heating rate: 20 °C/min.

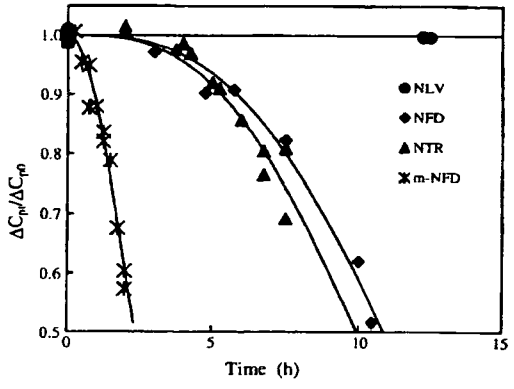

Fig. 3. Time profiles of crystallization for four dihydropyridines at 60 °C and 0%RH. The ratio of the amorphous form remaining at time t was calculated from the ΔC_p value assuming that the amount of amorphous phase is proportional to the ΔC_p. ΔC_{p0} and ΔC_{pt} are changes in ΔC_p at time 0 and t, respectively. Solid lines denote the fitting to the Avrami equation ($x(t) = \exp[-kt^n]$, $n = 3$).

Table 1
T_g values of amorphous NLV and NTR

RH (%)	T_g (°C)	
	NLV	NTR
0 (P_2O_5)	48.6 ± 0.3	32.4 ± 0.3
12 ($LiCl{\cdot}2H_2O$)	48.1 ± 0.7	30.5 ± 0.4
25 (CH_3COOK)	46.4 ± 0.5	29.0 ± 0.3
43 ($K_2CO_3{\cdot}2H_2O$)	43.4 ± 0.4	25.8 ± 0.3

For water absorption, the samples were kept at 5 °C for approximately 50 h in a desiccator containing saturated salt solutions. No crystallization was observed during the water absorption, as indicated by no endothermic melting peak in DSC thermograms.

(158 °C) and consistent with that reported for a metastable crystal (Kuhnert-Brandstätter and Völlenklee, 1986; Burger et al., 1997). As shown in Fig. 2(n) and (o), the partially crystallized NLV samples showed one melting peak at 148 °C. The observed melting point was lower than that for a stable crystal (168 °C) and similar to that for the dehydrated form of the monohydrate (Hirayama et al., 2000). Both amorphous NTR and NLV samples were considered to crystallize to their metastable crystalline forms under the conditions studied.

Fig. 3 shows the time profiles of crystallization of NFD, *m*-NFD, NTR, NLV at 60 °C and 0%RH. The crystallization rate was in the order: NLV < NTR = NFD < *m*-NFD. Fig. 4 shows the temperature dependence of the time required for 10% crystallization (t_{90}). Although NFD and NLV have approximately the same T_g, their values of t_{90} at the same temperature differed by more than two orders of magnitude (Fig. 4(A)). As shown in Fig. 4(B), the value of t_{90} at a given T_g/T (T being storage temperature) was in the order: NLV > NTR > NFD ≈ *m*-NFD within the whole range of temperature studied. As shown in Fig. 1, the four dihydropyridines have various alkyl groups at one of the carbonylester positions (R_2), and differ in the substitution position of the nitro group in the phenyl moiety (R_3 or R_4). The bulkiness of R_2 shows the order: NFD, *m*-NFD (methyl) < NTR (ethyl) < NLV (isopropyl). Furthermore, the substituent at R_1 is a cyano group in NLV, whereas it is a methyl group in the other three drugs; thus, the structural symmetry of NLV is lower. Since the plots for NFD and *m*-NFD in Fig. 4(B) almost overlapped each other, the difference in the crystallization rate may be attributed to the difference in molecular mobility. In contrast, differences in the crystallization rate between NLV, NTR and NFD cannot be explained only by the difference in molecular mobility. The differences in structural symmetry and bulkiness of functional group may cause differences in the Gibbs free energy and nucleus/amorphous interfacial energy, resulting in the differing crystallization rates between these drugs.

The crystallization rate of amorphous NLV and NTR solids with differing T_g values due to differing water content was measured to elucidate the effect of T_g on the crystallization rate (Table 1). The partially crystallized NLV and NTR in the presence of water showed an endothermic melting peak at approximately 150 °C and 130 °C, respectively. This suggests that amorphous NLV and NTR containing water also crystallize into their metastable forms in a similar manner as shown for dry samples. Fig. 5(A) shows the temperature dependence of the t_{90} obtained for NLV and NTR in the presence of water. When compared at the same temperature, the t_{90} value decreased with increasing RH. As shown in Fig. 5(B), the t_{90} versus T_g/T plots for each drug overlapped with those obtained under dry conditions, suggesting that the effect of water on the t_{90} value was explainable by the plasticizing effect of absorbed water,

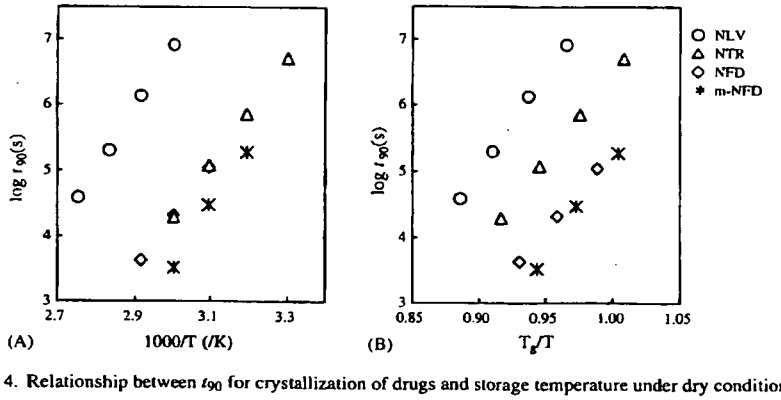

Fig. 4. Relationship between t_{90} for crystallization of drugs and storage temperature under dry conditions.

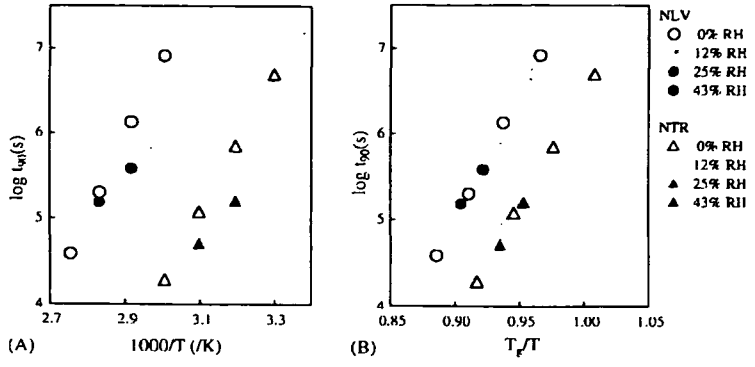

Fig. 5. Effect of absorbed water on the t_{90} of crystallization for NLV (circles) and NTR (triangles). The t_{90} values were measured at the early stage of crystallization at which no marked change in Tg was evident.

Table 2
T_g values of NTR-polymer solid dispersions

Polymer (%)	T_g (°C)	
	PVP	HPMC
0	32.4 ± 0.3	
3	33.2 ± 0.2	32.4 ± 0.1
5	34.1 ± 0.3	32.9 ± 0.4
6	34.1 ± 0.3	32.8 ± 0.2
11	36.6 ± 0.3	33.4 ± 0.3
20	–	33.7 ± 0.7
23	43.4 ± 0.8	–

similarly to that reported for NFD crystallization (Aso et al., 1995).

The effect of T_g on the crystallization rate of NTR was also investigated in solid dispersions with PVP and HPMC. A single T_g was observed for amorphous NTR-polymer solid dispersions prepared with 2.7–23% polymer excipients, indicating that NTR and polymer are miscible within the sensitivity limit of the DSC method. The value of T_g tended to increase with the amount of polymer, and the extent of increase was greater for NTR-PVP dispersions than for NTR-HPMC dispersions (Table 2). As the partially crystallized NTR-polymer dispersions showed a melt-

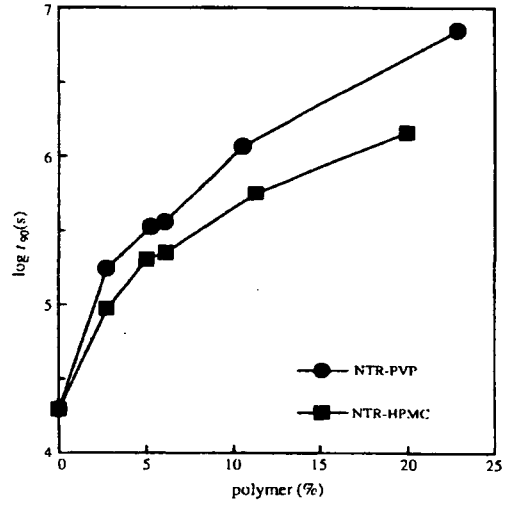

Fig. 6. Effect of polymer content on crystallization of NTR in solid dispersions with PVP and HPMC at 60 °C and 0%RH.

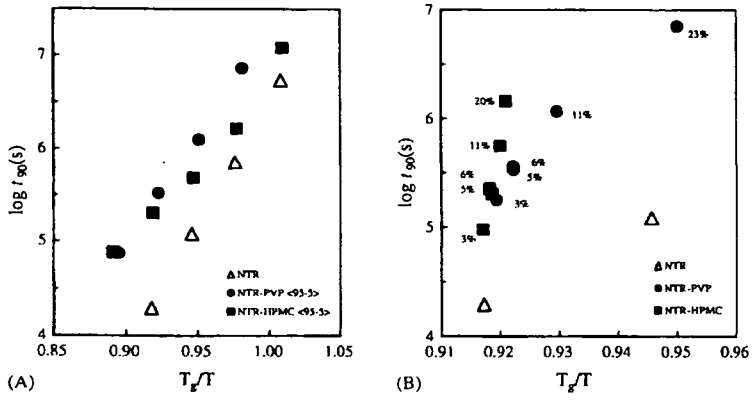

Fig. 7. Relationship between T_g/T and t_{90} of crystallization for NTR in the pure amorphous form and solid dispersions with PVP and HPMC. Numbers in percentage terms in figure (B) denote polymer contents.

ing peak at approximately 130 °C, the crystallization of NTR in the presence of the polymers was considered to be transition into a metastable form in a similar manner as that observed for pure amorphous NTR. Fig. 6 shows the effect of polymer excipients on the t_{90} values. Both PVP and HPMC increased t_{90} as the amount of polymer increased, but PVP was more effective in stabilizing amorphous NTR within the range of content studied. Fig. 7(A) shows the temperature dependence of t_{90} for solid dispersions containing 5% polymer. The t_{90} value compared at the same T_g/T was longer for both NTR-polymer dispersions than for pure NTR. Furthermore, the t_{90} versus T_g/T plots for solid dispersions containing various amounts of polymers did not overlap with that for pure NTR (Fig. 7(B)), indicating that crystallization of NTR was inhibited by the addition of PVP and HPMC to a greater extent than expected from the increased T_g. The present results imply that the drug-polymer interaction as well as an antiplasticizing effect of polymer excipients retarded the crystallization of the amorphous solid (Hirasawa et al., 2003a,b, 2004; Aso et al., 2004; Miyazaki et al., 2004, 2006; Wang et al., 2006).

Acknowledgement

A part of this work was supported by a grant from the Japan Health Science Foundation.

References

Andronis, V., Zografi, G., 2000. Crystal nucleation and growth of indomethacin polymorphs from the amorphous state. J. Non-Cryst. Solids 271, 236–248.

Aso, Y., Yoshioka, S., Otsuka, T., Kojima, S., 1995. The physical stability of amorphous nifedipine determined by isothermal microcalorimetry. Chem. Pharm. Bull. 43, 300–303.

Aso, Y., Yoshioka, S., Kojima, S., 2001. Explanation of the crystallization rate of amorphous nifedipine and Phenobarbital from their molecular mobility as measured by ^{13}C nuclear magnetic resonance relaxation time and the relaxation time obtained from the heating rate dependence of the glass transition temperature. J. Pharm. Sci. 90, 798–806.

Aso, Y., Yoshioka, S., Kojima, S., 2004. Molecular mobility-based estimation of the crystallization rates of amorphous nifedipine and Phenobarbital in poly(vinylpyrrolidone) solid dispersions. J. Pharm. Sci. 93, 384–391.

Burger, A., Koller, K.T., 1996. Polymorphism and pseudopolymorphism on nifedipine. Sci. Pharm. 64, 293–301.

Burger, A., Rollinger, J.M., Brüggeller, P., 1997. Binary system of (*R*)- and (*S*)-nitrendipine—polymorphism and structure. J. Pharm. Sci. 86, 674–679.

Hancock, B.C., Zografi, G., 1997. Characteristics and significance of the amorphous state in pharmaceutical systems. J. Pharm. Sci. 86, 1–12.

Hirasawa, N., Ishise, S., Miyata, H., Danjo, K., 2003a. Physicochemical characterization and drug release studies of Nilvadipine solid dispersions using water-insoluble polymer as a carrier. Drug Dev. Ind. Pharm. 29, 339–344.

Hirasawa, N., Ishise, S., Miyata, H., Danjo, K., 2003b. An attempt to stabilize Nilvadipine solid dispersion by the use of ternary systems. Drug Dev. Ind. Pharm. 29, 997–1004.

Hirasawa, N., Ishise, S., Miyata, H., Danjo, K., 2004. Application of Nilvadipine solid dispersion to tablet formulation and manufacturing using crospovidone and methylcellulose as dispersion carriers. Chem. Pharm. Bull. 52, 244–247.

Hirayama, F., Honjo, M., Arima, H., Okimoto, K., Uekama, K., 2000. X-ray crystallographic characterization of Nilvadipine monohydrate and its phase transition behavior. Eur. J. Pharm. Sci. 11, 81–88.

Kuhnert-Brandstätter, M., Völlenklee, R., 1986. Beitrag zur polymorphie von arzneistoffen 2. Mitteilung: halofenat, lorcainidhydrochlorid, minoxidil, mopidamol und nitrendipin. Sci. Pharm. 54, 71–82.

Miyazaki, T., Yoshioka, S., Aso, Y., Kojima, S., 2004. Ability of polyvinylpyrrolidone and polyacrylic acid to inhibit the crystallization of amorphous acetaminophen. J. Pharm. Sci. 93, 2710–2717.

Miyazaki, T., Yoshioka, S., Aso, Y., 2006. Physical stability of amorphous acetanilide derivatives improved by polymer excipients. Chem. Pharm. Bull. 54, 1207–1210.

Ngai, K.L., Magill, J.H., Plazek, D.J., 2000. Flow, diffusion and crystallization of supercooled liquids: revisited. J. Chem. Phys. 112, 1887–1892.

Rodríguez-Hornedo, N., Murphy, D., 1999. Significance of controlling crystallization mechanisms and kinetics in pharmaceutical systems. J. Pharm. Sci. 88, 651–660.

Saleki-Gerhardt, A., Zografi, G., 1994. Non-isothermal and isothermal crystallization of sucrose from the amorphous state. Pharm. Res. 11, 1166–1173.

Wang, L., Cui, F.D., Hayase, T., Sunada, H., 2005. Preparation and evaluation of solid dispersion for Nitrendipine-carbopol and Nitrendipine-HPMCP systems using a twin screw extruder. Chem. Pharm. Bull. 53, 1240–1245.

Wang, L., Cui, F.D., Sunada, H., 2006. Preparation and evaluation of solid dispersions of Nitrendipine prepared with fine silica particles using the melt-mixing method. Chem. Pharm. Bull. 54, 37–43.

Zhou, D., Zhang, G.G.Z., Law, D., Grant, K.J.W., Schmitt, E.A., 2002. Physical stability of amorphous pharmaceuticals: importance of configurational thermodynamic quantities and molecular mobility. J. Pharm. Sci. 91, 1863–1872.

J Pharmacol Sci 104, 397 – 401 (2007)

Journal of Pharmacological Sciences
©2007 The Japanese Pharmacological Society

Short Communication

Involvement of Intracellular Ca^{2+} in the Regulatory Volume Decrease After Hyposmotic Swelling in MDCK Cells

Naoko Iida-Tanaka[1], Iyuki Namekata[2], Megumi Kaneko[1], Miku Tamura[2], Toru Kawanishi[3], Ryu Nakamura[4], Koki Shigenobu[2], and Hikaru Tanaka[2,*]

[1]*Department of Food Science, Faculty of Home Economics, Otsuma Woman's University, Chiyoda-ku, Tokyo 102-8357, Japan*
[2]*Department of Pharmacology, Toho University Faculty of Pharmaceutical Sciences, Funabashi, Chiba 274-8510, Japan*
[3]*Division of Drugs, National Institute of Health Sciences, Setagaya-ku, Tokyo 158-8501, Japan*
[4]*Advanced Imaging Microscopy Department, Product Management Division of Microscopy, Carl Zeiss Tokyo, Shinjuku-ku, Tokyo 160-0003, Japan*

Received January 24, 2007; Accepted June 14, 2007

Abstract. We examined the source of Ca^{2+} involved in the volume regulation of Madin-Darby canine kidney (MDCK) cells with confocal microscopy and fluoroprobes. Hyposmosis induced a transient increase in cell volume, as well as cytoplasmic Ca^{2+}, which peaked at 3 to 5 min and gradually decreased to reach the initial value within about 30 min. This late decrease in cell volume, as well as the transient rise in cytoplasmic Ca^{2+}, was reduced in Ca^{2+}-free solution and was abolished by pretreatment with thapsigargin. In conclusion, Ca^{2+} released from the intracellular store contributes to the regulatory volume decrease following hyposmotic swelling in MDCK cells.

Keywords: hyposmosis, cell volume, intracellular Ca^{2+}

Although the composition of blood plasma is strictly regulated under physiological conditions, the cells in the body may experience anisosmolarity under pathological conditions such as ischemia, septic shock, and diabetic coma. The ability of cells to restore cell volume under such a condition may be crucial to their survival. Cells of various organs in the body including the heart, brain, kidney, bladder, liver, and skeletal muscle possess mechanisms for restoring cell volume under osmotic challenge and can reverse the swelling effect of hyposmosis and the shrinking effect of hyperosmosis (1).

Madin-Darby canine kidney (MDCK) cells originate from the renal distal tubular epithelium. In this cell line, the key players of water and ion transport such as aquaporins and ion channels are expressed (2, 3), and responsiveness to humoral regulatory substances such as vasopressin is well maintained (4). Thus, MDCK cells have been widely used as a model to study volume regulation of renal epithelial cells. We have reported that over-expression of sulfoglycolipids confers resistance against hyper- and hypotonic stresses to MDCK cells (5). Following hyposmotic challenge, the volume of MDCK cells are known to increase within a few minutes, which is followed by a decrease towards the initial value under hyposmotic conditions (6, 7), a process known as regulatory volume decrease (8, 9). Activation of ion channels such as potassium and chloride channels have been reported and some of these processes are postulated to be triggered by a rise in cytoplasmic Ca^{2+} concentration. However, the source of Ca^{2+} responsible for the rise has not been clarified. In the present study, we performed measurements of the cell volume and cytoplasmic Ca^{2+} in MDCK cells by confocal and epifluorescent microscopy to determine the significance and source of Ca^{2+} in the regulatory volume decrease under persistent hyposmotic conditions.

MDCK cells (National Institute of Health Science) were cultured in Eagles Modified Essential Medium (EMEM) supplemented with 1% penicillin and 0.4% streptomycin. The transformants were plated on glass coverslips 48 to 72 h before the experiments. At 1 h before the experiments, the coverslips were placed in a

*Corresponding author. htanaka@phar.toho-u.ac.jp
Published online in J-STAGE: August 10, 2007
doi: 10.1254/jphs.SC0070024

recording chamber containing the culture medium and loaded with the Ca^{2+}-sensitive fluoroprobe Fluo 3 or Indo 1 and/or the membrane staining fluoroprobe PKH67 or PKH26 (Sigma-Aldrich, St. Louis, MO, USA). The Ca^{2+}-sensitive probes were loaded using the acetoxymethyl derivative Fluo 3-AM or Indo 1-AM (Dojin, Kumamoto) at a concentration of 10 μM. The membrane probes were dissolved in the loading buffer supplied by the manufacturer and applied to the cells at a final concentration of 5 μM. Then the coverslips with cells were placed in a chamber on the stage of the inverted microscopes and perfused with the normal culture medium as described above to washout the excess fluorescent probes. In the case of hyposmosis under the Ca^{2+}-free extracellular condition, the cells were treated with Ca^{2+} free solution from 30 min before hyposmosis. All the experiments were performed at 37°C.

Confocal imaging of membrane-labeled MDCK cells was performed with LSM510 as in our previous study (10) or with LSM5 *LIVE* (Carl Zeiss, Jena, Germany). The cells were excited at 488 or 543 nm from an Ar^{+} laser and the emission at wavelengths between 500 and 530 nm or longer than 560 nm, respectively, was detected by photo multipliers. The data obtained were assembled into three-dimentional or two-dimentional (x-z) images. The objective used was Plan-Apocromat 63x/1.4 NA oil immersion (Carl Zeiss).

Changes in intracellular Ca^{2+} concentration of MDCK cells loaded with Indo 1 were determined by epifluorescent microscopy. The microscope was IX-70 (Olympus, Tokyo) and the objective was UApocromat 40x/340 water immersion (Olympus). The cells were excited at 360 nm from a Xenon lamp and the emission bands, 395 to 415 nm and 470 to 490 nm, were separated (W-VIEW system; Hamamatsu Photonics, Hamamatsu), detected by a high-speed cooled CCD camera (C6790, Hamamatsu Photonics), and ratioed after correction of background fluorescence (Aquacosmos software, Hamamatsu Photonics) as in our previous studies (11, 12).

The osmolarity of the basic culture medium was 300 mOsm as determined by a freezing point-based osmometer. The NaCl concentration was reduced by 100 mM in the hyposmotic media, whose osmolarity was confirmed to be 100 mOsm. After the cells were equilibrated for 30 min in normal or Ca^{2+}-free medium in the absence or presence of 1 μM thapsigargin, the perfusate was changed from to the hyposmotic medium.

All data are expressed as means ± S.E.M. Data were analyzed by one-way analysis of variance followed by Dunnett's multiple test, and a P value less than 0.05 was considered statistically significant.

The cell membrane was clearly stained with the fluorescent dye PKH67 and the hyposmosis-induced cell swelling could be visualized in three-dimensional images (Fig. 1A). Simultaneous staining of the cells with PKH26 and Fluo 3 enabled simultaneous measurement of cell volume and cytoplasmic Ca^{2+} (Fig. 1: B and C). Hyposmosis induced a transient increase in cell volume, which peaked at 3 – 10 min and gradually decreased to the reach initial value within about 20 min. The Fluo 3-fluorescence showed a triphasic change: an initial decrease was followed by a transient increase that peaked at 3 – 10 min, and finally a sustained decrease was observed. The late decrease in cell volume, as well as the transient rise in Fluo 3-fluorescence, was partly reduced in Ca^{2+}-free extracellular media, and it was abolished by pretreatment of the cells with thapsigargin.

To analyze the changes in cytoplasmic Ca^{2+} and cell volume upon hyposmotic challenge more quantitatively, the Ca^{2+} concentration was measured by epifluorescent microscopy (Fig. 2: A and B) and the ratiometric probe Indo 1, and the cell volume was analyzed from x-z sections with confocal microscopy (Fig. 2C). The possible decrease in intracellular Ca^{2+} mentioned above could not be observed in Indo 1-loaded cells (Fig. 2A), which indicates that the observed decrease in Fluo 3-fluorescence could be the result of dye dilution as a result of cell volume increase. The increase in cytoplasmic Ca^{2+} was partially reduced in Ca^{2+}-free extracellular media and was significantly abolished by pretreatment with 1 μM thapsigargin. The increase in cell volume after hyposmotic challenge was affected neither by the absence of extracellular Ca^{2+} nor by pretreatment with thapsigargin (Fig. 2C). The volume decrease following the initial swelling was significantly reduced by pretreatment with 1 μM thapsigargin ($P<0.01$) irrespective of the presence or absence of extracellular Ca^{2+} during measurement. The decrease in cell volume expressed as a percentage of the initial increase in each cell was 89.1 ± 4.1% in control cells, 74.4 ± 14.9% under Ca^{2+}-free extracellular media, 14.12 ± 11.2% in thapsigargin-pretreated cells, and 23.3 ± 7.2% in thapsigargin-pretreated cell under Ca^{2+}-free extracellular media (data from 13 – 16 cells for each group).

The effect of treatment with Ca^{2+}-free extracellular solution on intracellular releasable Ca^{2+} was evaluated with caffeine. The cells were treated with Ca^{2+}-free extracellular solution for different time periods and then 20 mM caffeine was applied. The caffeine-induced peak Ca^{2+} concentration after treatment with Ca^{2+}-free extracellular solution for 0, 10, 30, and 60 min was 722.0 ± 50.5, 410.0 ± 65.3, 262.6 ± 23.7, and 140.8 ± 23.0 nM (data from 20 cells for each group), respectively.

Application of hyposmotic shock to the MDCK cells

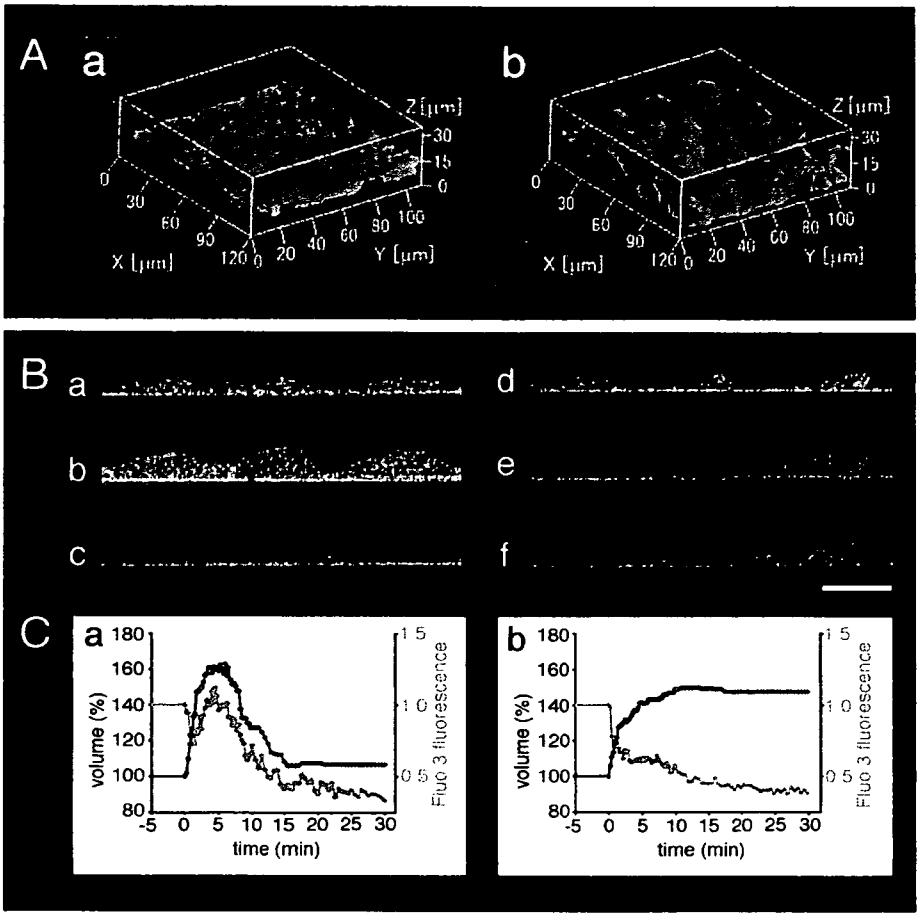

Fig. 1. Changes in cell volume and cytoplasmic Ca^{2+} during hyposmotic shock. A: Typical three-dimensional images of MDCK cells under normal osmolarity (a) and at the peak of cell swelling under the hyposmotic condition (b). The cell membrane was stained with PKH67 and excited at 488 nm. Images were obtained with the line-scan mode of LSM5 *LIVE*. Each x-y image in a single confocal plane was obtained in 56.6 ms, and the distance between confocal planes in the z-direction was 0.6 μm. A total of 52 confocal planes were scanned in 2.9 s to construct each 3-d image. B: Typical x-z images of MDCK cells untreated (a, b, c) and pretreated with 1 μM thapsigargin (d, e, f). The images were obtained under normal osmolarity (a, d), at 5 min after hyposmotic shock (b, e), and at 30 min after hyposmotic shock (c, f). The cells were stained with the membrane probe PKH26 and the Ca^{2+} probe Fluo 3 and excited at 543 and 488 nm consecutively under the multi-track mode of LSM510. The fluorescence of PKH26 and Fluo 3 were shown in red and green, respectively, and merged. The horizontal bar indicates 10 μm. C: Typical time course of changes in cell volume and cytoplasmic Ca^{2+}. The area of the cell in x-z sections was used as an index of cell volume, which was expressed as a percentage of the value under normoxic condition. Fluo 3-fluorescence was also normalized with the value under normal osmolarity (time zero).

induced an increase in cell volume followed by a decrease towards the initial value under persistent hyposmolarity, a process known as regulatory volume decrease. The initial swelling was accompanied by an increase in cytoplasmic Ca^{2+} concentration, a phenomenon observed in this cell line by other investigators (6, 7) and also in other cell lines of renal epithelial origin (8). This increase in cytoplasmic Ca^{2+} was partly reduced under Ca^{2+}-free extracellular solution. Although the simplest interpretation is that the increase in Ca^{2+} resulted from activation of Ca^{2+} influx across the cell membrane (6), involvement of intracellular Ca^{2+} release cannot be excluded because treatment of cells with Ca^{2+}-free solution often results in depletion of intracellular Ca^{2+} store sites. In fact, the present experiments with caffeine proved that intracellular Ca^{2+} was indeed gradually decreased during treatment with Ca^{2+}-free extracellular solution under the present experimental conditions: the releasable intracellular Ca^{2+} was decreased by more than 60% after 30 min. Furthermore, the hyposmosis-induced rise in cytoplasmic Ca^{2+} was completely inhibited by thapsigargin, which is widely

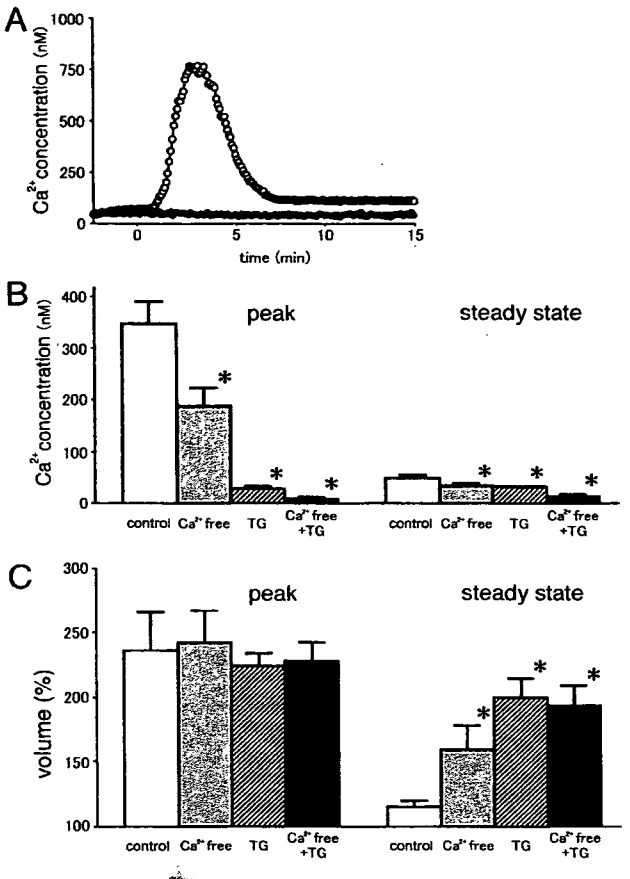

Fig. 2. Cell volume and cytoplasmic Ca^{2+} during hyposmotic shock. A: Typical time course of changes in intracellular Ca^{2+} concentration calculated from Indo I fluorescence ratio in control cells (open circles) and cells pretreated with 1 μM thapsigargin (closed circles). Hyposmotic shock was applied at time zero. B: Summarized results for the peak and steady state intracellular Ca^{2+} concentration in Indo I-loaded cells under normal condition (control: open columns), under Ca^{2+}-free condition (gray columns), in cells pretreated with thapsigargin (hatched columns), and in cells pretreated with thapsigargin under Ca^{2+}-free condition (closed columns). Data are presented as the mean ± S.E.M. from 25 – 31 cells. C: Summarized results for the peak and steady state cell volume in cells labeled with PKH67 under normal condition (control: open columns), under Ca^{2+}-free condition (gray columns), in cells pretreated with thapsigargin (hatched columns), and in cells pretreated with thapsigargin under Ca^{2+}-free condition (closed columns). Cell volume was expressed as a percentage of the initial value before hyposmotic shock. Data are presented as the mean ± S.E.M. from 13 – 16 cells. Asterisks indicate significant difference from control values, $P<0.05$.

used as a depleter of the endoplasmic reticulum Ca^{2+} store (Figs. 1 and 2). This indicates that release from intracellular store sites largely contributes to the hyposmosis-induced rise in cytoplasmic Ca^{2+} concentration. Concerning the mechanisms triggering the Ca^{2+} release, one of the possibilities is the IP3-induced release from the endoplasmic reticulum. Stimulation by agonists of MDCK cells was reported to result in production of inositol phosphate and release of Ca^{2+} from intracellular stores (13). Translocation of phospholipase C following hyposmotic shock was also observed in MDCK cells, which may be a mechanism to trigger Ca^{2+} release from the endoplasmic reticulum through production of IP3 (14).

Although the details of the regulatory volume decrease mechanism remains to be investigated, many reports suggest the involvement of osmolyte efflux through potassium and chloride channels. Some researchers postulate that these channels are activated by the decrease in intracellular ionic strength on swelling (15). On the other hand, these ion channels are activated by an increase in intracellular Ca^{2+} concentration. In the present study, the magnitude of the volume decrease under different conditions correlated with the magnitude of the transient increase in cytoplasmic Ca^{2+} concentration. This indicates that the increase in cytoplasmic Ca^{2+} concentration plays a significant role in the regulatory volume decrease following hyposmotic shock in MDCK cells.

In conclusion, the present results suggested that Ca^{2+} released from the intracellular store contributes to the regulatory volume decrease following hyposmotic swelling in MDCK cells.

Acknowledgments

This study was supported in part by a grant-in-aid for Drug Innovation Science Project to T.K. and K.S. from the Japan Health Science Foundation. This study was performed as a part of the project "Research on the molecular mechanisms of appearance of age-related diseases by failure of cell function control system, and their prevention and treatment" by the "Research Center for Aging and Age-related Diseases" established in the Toho University Faculty of Pharmaceutical Sciences.

References

1 MacKnight A, Leaf A. Regulation of cellular volume. Physiol Rev. 1977;57:510–572.
2 Volkl H, Paulmichl M, Lang F. Cell volume regulation in renal cortical cells. Ren Physiol Biochem. 1988;11:158–173.
3 Takata K, Tajika Y, Matsuzaki T, Aoki T, Suzuki T, Abduxukur A, et al. Molecular mechanisms and drug development in aquaporin water channel diseases: water channel aquaporin-2 of kidney collecting duct cells. J Pharmacol Sci. 2004;96:255–259.
4 Simmons N. Cultured monolayers of MDCK cells: a novel model system for the study of epithelial development and function. Gen Pharmacol. 1982;13:287–291.
5 Suzuki C, Iida-Tanaka N, Nishizawa K, Honke K, Matsumoto I, Ishizuka I. [Sulfoglycolipid modifies p38 MAP kinase activation

by osmotic stress.] Seikagaku. 2003;75:781. (abstract in Japanese)

6 Rothstein A, Mack E. Volume-activated calcium uptake: its role in cell volume regulation of Madin-Darby canine kidney cells. Am J Physiol. 1992;262:C339–C347.

7 Woll E, Ritter M, Haller T, Volkl H, Lang F. Calcium entry stimulated by swelling of Madin-Darby canine kidney cells. Nephron. 1996;74:150–157.

8 Yu W, Sokabe M. Hypotonically induced whole-cell currents in A6 cells: relationship with cell volume and cytoplasmic Ca^{2+}. Jpn J Physiol. 1997;47:553–565.

9 Okada Y, Maeno E, Shimizu T, Dezaki K, Wang J, Morishima S. Receptor-mediated control of regulatory volume decrease (RVD) and apoptotic volume decrease (AVD). J Physiol. 2001;532:3–16.

10 Kawai H, Suzuki T, Kobayashi T, Sakurai H, Ohata H, Honda K, et al. Simultaneous real-time detection of initiator- and effector-caspase activation by double fluorescence resonance energy transfer analysis. J Pharmacol Sci. 2005;97:361–368.

11 Namekata I, Kawanishi T, Iida-Tanaka N, Tanaka H, Shigenobu K. Quantitative fluorescence measurement of cardiac Na^+/Ca^{2+} exchanger by kinetic analysis in stably transfected HEK293 cells. J Pharmacol Sci. 2006;101:356–360.

12 Tanaka H, Shimada H, Namekata I, Kawanishi T, Iida-Tanaka N, Shigenobu K. Involvement of the Na^+/Ca^{2+} exchanger in ouabain-induced inotropy and arrhythmogenesis in guinea-pig myocardium as revealed by SEA0400. J Pharmacol Sci. 2007;103:241–246.

13 Aboolian A, Vander Molen M, Nord E. Differential effects of phorbol esters on PGE2 and bradykinin-induced elevation of $[Ca^{2+}]i$ in MDCK cells. Am J Physiol. 1989;256:F1135–F1143.

14 Fujii M, Ohtsubo M, Ogawa T, Kamata H, Hirata H, Yagisawa H. Real-time visualization of PH domain-dependent translocation of phospholipase C-delta1 in renal epithelial cells (MDCK): response to hypo-osmotic stress. Biochem Biophys Res Commun. 1999;254:284–291.

15 Nilius B, Prenen J, Voets T, Eggermont J, Droogmans G. Activation of volume-regulated chloride currents by reduction of intracellular ionic strength in bovine endothelial cells. J Physiol. 1998;506:353–361.

Chem. Pharm. Bull. 55(8) 1227—1231 (2007)

Miscibility of Nifedipine and Hydrophilic Polymers as Measured by ^{1}H-NMR Spin–Lattice Relaxation

Yukio Aso,*[a] Sumie Yoshioka,[a] Tamaki Miyazaki,[a] Tohru Kawanishi,[a] Kazuyuki Tanaka,[b] Satoshi Kitamura,[b] Asako Takakura,[c] Takashi Hayashi,[c] and Noriyuki Muranushi[c]

[a] *National Institute of Health Sciences: 1–18–1 Kamiyoga, Setagaya-ku, Tokyo 158–8501, Japan:* [b] *Astellas Pharma Inc.: 180 Ozumi, Yaizu, Shizuoka 425–0072, Japan: and* [c] *Shionogi & Co., Ltd.; 2–1–3 Kuise, Terajima, Amagasaki, Hyogo 660–0813, Japan.* Received April 19, 2007; accepted June 4, 2007; published online June 5, 2007

The miscibility of a drug with excipients in solid dispersions is considered to be one of the most important factors for preparation of stable amorphous solid dispersions. The purpose of the present study was to elucidate the feasibility of ^{1}H-NMR spin–lattice relaxation measurements to assess the miscibility of a drug with excipients. Solid dispersions of nifedipine with the hydrophilic polymers poly(vinylpyrrolidone) (PVP), hydroxypropylmethylcellulose (HPMC) and α,β-poly(*N*-5-hydroxypentyl)-L-aspartamide (PHPA) with various weight ratios were prepared by spray drying, and the spin–lattice relaxation decay of the solid dispersions in a laboratory frame (T_1 decay) and in a rotating frame ($T_{1\rho}$ decay) were measured. $T_{1\rho}$ decay of nifedipine–PVP solid dispersions (3 : 7, 5 : 5 and 7 : 3) was describable with a mono-exponential equation, whereas $T_{1\rho}$ decay of nifedipine–PHPA solid dispersions (3 : 7, 4 : 6 and 5 : 5) was describable with a bi-exponential equation. Because a mono-exponential $T_{1\rho}$ decay indicates that the domain sizes of nifedipine and polymer in solid dispersion are less than several nm, it is speculated that nifedipine is miscible with PVP but not miscible with PHPA. All the nifedipine–PVP solid dispersions studied showed a single glass transition temperature (T_g), whereas two glass transitions were observed for the nifedipine–PHPA solid dispersion (3 : 7), thus supporting the above speculation. For nifedipine–HPMC solid dispersions (3 : 7 and 5 : 5), the miscibility of nifedipine and HPMC could not be determined by DSC measurements due to the lack of obviously evident T_g. In contrast, ^{1}H-NMR spin–lattice relaxation measurements showed that nifedipine and HPMC are miscible, since $T_{1\rho}$ decay of the solid dispersions (3 : 7, 5 : 5 and 7 : 3) was describable with a mono-exponential equation. These results indicate that ^{1}H-NMR spin–lattice relaxation measurements are useful for assessing the miscibility of a drug and an excipient in solid dispersions.

Key words miscibility; solid dispersion; spin diffusion; spin–lattice relaxation time; amorphous

Preparing solid dispersions of a poorly soluble drug with water-soluble polymers is a promising method for improving the dissolution characteristics and bioavailability of the drug. Miscibility between a drug and a polymer is considered to be one of the most important factors for obtaining stable solid dispersions.[1)]

Miscibility of a drug with a polymer is usually evaluated by differential scanning calorimetry (DSC).[2—6)] When a solid dispersion shows a single glass transition temperature (T_g) between the T_g values of the drug and the polymer, the drug and the polymer are considered to be miscible within the detection limit of DSC.[7)] This method is applicable to a solid dispersion when T_g of the drug and the polymer can be detected clearly, and the temperature ranges of the base line shift due to glass transition do not overlap each other.

The interaction parameter χ of the Flory–Huggins equation provides a measure of miscibility.[8,9)] Crowly and Zografi measured the water vapor sorption isotherm of indomethacin solid dispersions with PVP and reported that the estimated interaction parameter χ between indomethacin and PVP was greater than 0.5, indicating that indomethacin and PVP are immiscible in terms of χ value.[8)] Although this method is excellent in being able to provide a quantitative measure of miscibility, it may be difficult to apply to unstable amorphous drugs, which crystallize during measurement of water vapor sorption.

A method that can be used as an alternative to DSC or measurement of the interaction parameter χ is analysis of the ^{1}H spin–lattice relaxation process of solid dispersions, which has been reported in the fields of polymer alloy and polymer blends. If two polymers are miscible, the relaxation decay of the mixture is describable by a mono-exponential equation, whereas if they are not miscible, relaxation decay is describable by a bi-exponential equation.[10,11)]

In this paper, the feasibility of ^{1}H spin–lattice relaxation measurements for evaluating the miscibility of a drug and polymers in solid dispersions was studied. Nifedipine solid dispersions with PVP, HPMC and α,β-poly(*N*-5-hydroxypentyl)-L-aspartamide (PHPA) were used as model solid dispersions, and the miscibility measured by ^{1}H-NMR was compared with that measured by DSC. The dissolution profiles of nifedipine from PVP solid dispersions were compared with those from PHPA solid dispersions to discuss the effects of miscibility on the dissolution rate of nifedipine.

Theory ^{1}H spin–lattice relaxation rates of respective spins in a solid are usually averaged by a process called spin diffusion. Spin diffusion is the equilibration process of polarizations of spins at different local sites through mutual exchange of magnetization. ^{1}H spin–lattice relaxation decay for a single-phase solid is describable by a mono-exponential equation with a relaxation rate that is averaged by spin diffusion. When a solid consists of two phases, the spin–lattice relaxation decay is describable by a mono-exponential or a bi-exponential equation depending on both the domain size of each phase and the effective diffusion length (L). L is expressed as follows:

$$L=\sqrt{6Dt} \quad (1)$$

* To whom correspondence should be addressed. e-mail: aso@nihs.go.jp

© 2007 Pharmaceutical Society of Japan

where D is the spin diffusion coefficient, and t is the diffusion time. D is a function of the distance between neighboring proton spins and spin–spin relaxation time (T_2), and is reported to be approximately $10^{-12}\,cm^2\,s^{-1}$ for organic polymers. Typical spin–lattice relaxation time in a laboratory frame (T_1) and that in a rotating frame ($T_{1\rho}$) are of the order of 1 s and 10 ms, respectively. When these values for t were inserted in Eq. 1, effective diffusion lengths of approximately 50 nm and 5 nm were obtained for T_1 and $T_{1\rho}$, respectively. Depending on the domain size of each phase in a solid, the following 3 cases can be expected: (1) when the domain is smaller than about 5 nm, both the spin–lattice relaxation decay patterns in a laboratory frame (T_1 decay) and in a rotating frame ($T_{1\rho}$ decay) are describable by a mono-exponential equation; (2) when the domain size is about 5 to 50 nm, the $T_{1\rho}$ decay pattern is describable by a bi-exponential equation, whereas the T_1 decay pattern is describable by a mono-exponential equation; and (3) when the domain size is larger than about 50 nm, both the T_1 and $T_{1\rho}$ decay patterns are describable by a bi-exponential equation. When the $T_{1\rho}$ decay is describable by a mono-exponential equation, the solid can be considered as a single phase within the detection limit of NMR. T_1 and $T_{1\rho}$ decay thus provide information on miscibility of a drug and a polymer excipient.[11]

Experimental

Materials Nifedipine (N-7634), PVP (PVP-40) and HPMC (H-3785) were purchased from Sigma (Newcastle, DE, U.S.A.). PHPA was synthesized *via* polycondensation of L-aspartic acid.[12] Phenobarbital was obtained from sodium phenobarbital (Wako Pure Chemical Ind., Osaka) by neutralization and subsequent re-crystallization from acetone solutions as described previously.[13] Other chemicals used were of reagent grade. Nifedipine solid dispersions with PVP, HPMC and PHPA were prepared by a solvent evaporation method using a model GS-310 spray dryer (Yamato, Tokyo, Japan). Drying conditions are summarized in Table 1. The solid dispersions obtained were confirmed to be amorphous from microscopic observation under polarized light. Although the drying conditions were not optimized, 50 to 90% of the solid dispersions were obtained. Amorphous nifedipine was prepared by melting and subsequent rapid cooling as reported previously.[14]

DSC T_g of nifedipine–PVP and nifedipine–HPMC solid dispersions was measured by modulated temperature DSC using a model 2920 differential scanning calorimeter and a refrigerator cooling system (TA Instruments, Newcastle, DE, U.S.A.). The modulated temperature program used was a modulation amplitude of ± 0.5 °C, a modulation period of 100 s and an underlying heating rate of 1 °C/min. For nifedipine–PHPA solid dispersions, T_g was measured at a scanning rate of 20 °C/min using a conventional heating program. Temperature calibration of the instrument was carried out using indium.

NMR T_1 decay and $T_{1\rho}$ decay were measured using a model JNM-MU25 pulsed NMR spectrometer (JEOL DATUM, Tokyo, Japan). The inversion recovery pulse sequence was used to measure T_1 decay. $T_{1\rho}$ decay was measured in a spin locking field of 10 G. All measurements were carried out at 27 °C.

X-Ray Powder Diffraction X-Ray powder diffraction patterns of solid dispersions were obtained using a model RINT-TTR II X-ray diffractometer (Rigaku Denki, Tokyo) with Cu$K\alpha$ radiation (50 kV, 300 mA) at a scanning rate of 4 °C/min from $2\theta = 5°$ to 40°.

Nifedipine Dissolution Profile Nifedipine–PVP (3 : 7) and nifedipine–PHPA (3 : 7) solid dispersions containing 100 mg of nifedipine were made into disks with a diameter of 2 cm at a pressure of 20 kN. Each disk was mounted on the rotor of the dissolution apparatus and the side surface of the disk was covered with a Teflon film. The sample was rotated at a rate of 100 rpm in 900 ml of distilled water at 37 °C. The amount of nifedipine dissolved was measured using a model DM-3100 solution monitor (Otsuka Electronics, Tokyo).

Results and Discussion

Figure 1 shows typical T_1 and $T_{1\rho}$ decay patterns for the solid dispersion and the physical mixture of nifedipine and PHPA (3 : 7). T_1 and $T_{1\rho}$ decay patterns were mono-exponential for both amorphous nifedipine and PHPA. The T_1 and $T_{1\rho}$ values of nifedipine were 5.0 s and 104 ms, respectively, and those of PHPA were 0.084 s and 4.4 ms, respectively. The physical mixture of nifedipine and PHPA (3 : 7) exhibited bi-exponential T_1 and $T_{1\rho}$ decay with the relaxation time of each component, indicating that the particle sizes of nifedipine and PHPA in the physical mixture are much larger than the effective diffusion length (approximately 5 nm and 50 nm for $T_{1\rho}$ and T_1 decay, respectively). In contrast to the physical

Table 1. Conditions of Spray Drying

Drug	Polymer	Solvent[a]	Outlet temperature (°C)	Atomizer gas (l/min)	Feeding rate (ml/min)
Nifedipine–PHPA					
0	10	A	68	7	5
3	7	A	68	7	3
4	6	A	68	7	3
5	5	A	68	7	3
Phenobarbital–PHPA					
3	7	A	68	7	3
Nifedipine–PVP					
0	10	A	90	9	10
3	7	A	90	9	10
5	5	A	90	9	10
7	3	A	68	7	3
Nifedipine–HPMC					
0	10	B	38	11	3
3	7	B	38	11	2
5	5	B	38	11	2
7	3	B	38	11	4

a) Solvent A, ethanol; solvent B, ethanol–CH_2Cl_2 (1 : 1). Flow rate of drying gas was adjusted to 0.5 m^3/min.

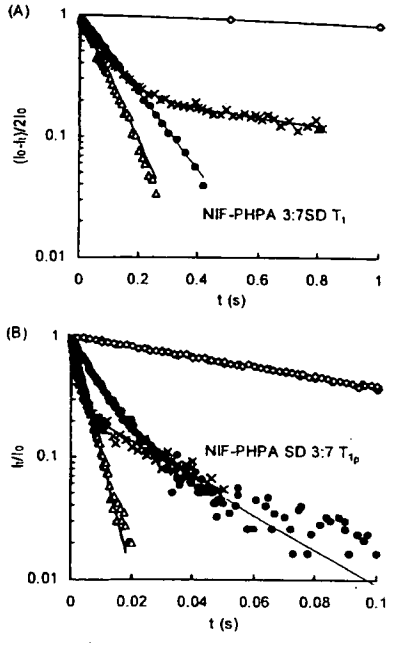

Fig. 1. T_1 (A) and $T_{1\rho}$ (B) Decay Patterns for Amorphous Nifedipine (◇), Amorphous PHPA (△), Physical Mixture (×) and Solid Dispersions (●) of Nifedipine and PHPA

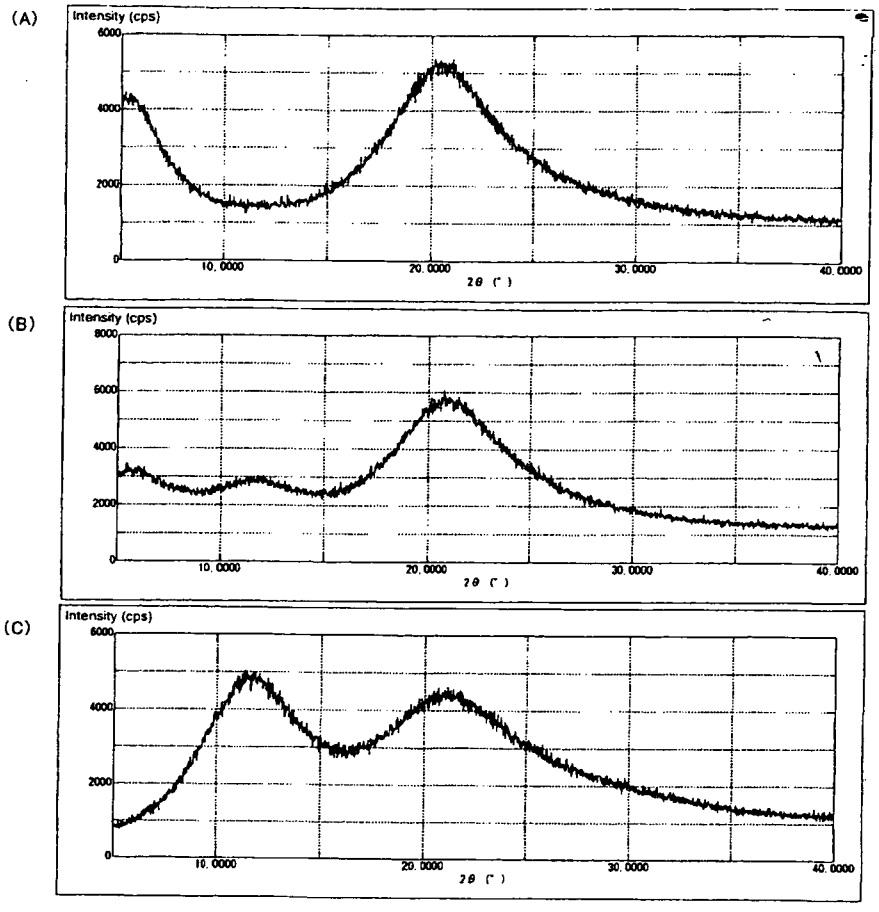

Fig. 2. Powder X-Ray Diffraction Patterns of PHPA (A), Nifedipine–PHPA (3 : 7) (B) and Nifedipine–PVP Solid Dispersions (3 : 7) (C)

mixture, the solid dispersion (3 : 7) showed mono-exponential T_1 decay, whereas bi-exponential $T_{1\rho}$ decay. These results indicate that nifedipine and PHPA are immiscible and that domains 5 to 50 nm in size are present in the solid dispersion. The nifedipine–PHPA solid dispersions (4 : 6 and 5 : 5) and the phenobarbital–PHPA solid dispersions (3 : 7) also exhibited bi-exponential $T_{1\rho}$ decay (data not shown). Figure 2 shows powder X-ray diffraction patterns of the nifedipine–PHPA and nifedipine–PVP solid dispersions. The observed halo pattern indicates that nifedipine in the PHPA dispersions is amorphous at the detection limit of powder X-ray diffractometry.

DSC data supported the contention that nifedipine and PHPA are immiscible. Figure 3 shows typical DSC traces for nifedipine–PHPA solid dispersions. The nifedipine–PHPA solid dispersion (3 : 7) showed glass transition at approximately 50 °C, corresponding to the T_g of amorphous nifedipine, and at approximately 75 °C, indicating that there are both an amorphous nifedipine phase and an amorphous nifedipine–PHPA phase in the solid dispersion. These DSC data indicate that amorphous nifedipine and PHPA are partially immiscible at this weight ratio. For the nifedipine–PHPA solid dispersion (5 : 5), T_g of the amorphous nifedipine–PHPA phase was not clearly observed because of the detection limit of DSC, suggesting that ^{1}H-NMR relaxation measurements can detect immiscibility of drugs and polymers more sensitively than DSC. DSC data suggest that the nifedipine–PHPA solid dispersion (3 : 7) consists of pure amorphous nifedipine phase and amorphous nifedipine–PHPA phase. NMR data may support this speculation. As shown in Fig. 1B, initial $T_{1\rho}$ decay of the solid dispersion was slower than that of the physical mixture or pure PHPA. This slow relaxation rate of the solid dispersion may indicate that the relaxation rate of PHPA protons was decreased by spin diffusion with nifedipine protons existing near PHPA molecules; in other words, nifedipine–PHPA phase is considered to exist in the solid dispersion. The effect of weight ratios on the $T_{1\rho}$ decay of nifedipine–PHPA solid dispersions needs to examine in order

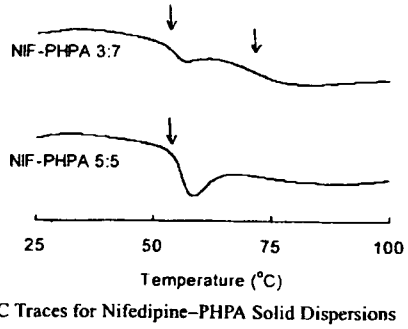

Fig. 3. DSC Traces for Nifedipine–PHPA Solid Dispersions
Arrows represent T_g.